应用数学和力学
APPLIED MATHEMATICS AND MECHANICS

变截面二维功能梯度微梁的振动和屈曲特性

雷 剑，谢宇阳，姚明格，何玉明

Vibration and Buckling Characteristics of 2D Functionally Graded Microbeams With Variable Cross Sections

LEI Jian, XIE Yuyang, YAO Mingge, and HE Yuming

在线阅读 View online: https://doi.org/10.21656/1000-0887.420323

http://www.applmathmech.cn

变截面二维功能梯度微梁的振动和屈曲特性*

雷　剑[1]，　谢宇阳[1]，　姚明格[2]，　何玉明[1]

（1. 华中科技大学 航空航天学院，武汉 430074；
2. 天津航天瑞莱科技有限公司，武汉 430056）

摘要：　基于修正的偶应力理论和 Timoshenko 梁理论，应用变分原理建立了变截面二维功能梯度微梁的自由振动和屈曲力学模型. 模型中包含金属组分和陶瓷组分的材料内禀特征尺度参数，可以预测微梁力学行为的尺度效应. 采用 Ritz 法给出了任意边界条件下微梁振动频率和临界屈曲载荷的数值解. 数值算例表明：微梁厚度减小时，无量纲一阶频率和无量纲临界屈曲载荷增大，尺度效应增强. 锥度比对微梁一阶频率的影响与边界条件密切相关，同时，对应厚度和对应宽度锥度比的影响也有明显差异. 变截面微尺度梁无量纲一阶频率随着陶瓷和金属的材料内禀特征尺度参数比的增加而增大，且不同边界条件时增大程度不同. 厚度方向和轴向功能梯度指数对微梁的一阶频率和屈曲载荷也有显著的影响.

关　键　词：　修正的偶应力理论；　功能梯度材料；　变截面梁；　尺度效应；　振动和屈曲

中图分类号：　O341　　**文献标志码：**　A　　DOI：10.21656/1000-0887.420323

Vibration and Buckling Characteristics of 2D Functionally Graded Microbeams With Variable Cross Sections

LEI Jian[1]，　XIE Yuyang[1]，　YAO Mingge[2]，　HE Yuming[1]

（1. *School of Aerospace Engineering*, *Huazhong University of Science and Technology*, *Wuhan* 430074, *P.R.China*；
2. *Tianjin Aerospace Reliability Technology Co. Ltd.*, *Wuhan* 430056, *P.R.China*）

Abstract: Based on the modified couple stress theory and the Timoshenko beam theory, the free vibration and buckling mechanics model for 2D functionally graded microbeams with variable cross sections was established by means of the variational principle. The model contains the intrinsic material length scale parameters of the metal and ceramic components, which can predict the size effects of microbeams. The Ritz method was used to obtain the numerical solution of the vibration frequencies and critical buckling loads of the microbeams under arbitrary boundary conditions. Numerical examples reveal that, when the thickness of the microbeam decreases, the dimensionless 1st-order frequency and the dimensionless critical buckling load will increase, and the scale effect will grow larger. The effect of the taper ratio on the dimensionless 1st-order frequency of the microbeam is closely related to the boundary conditions. At the same time, the effects of the taper ratios of the thickness and the width are also significantly different. The dimensionless 1st-order frequencies of microbeams increase with the material length scale parameter ratios of ceramic and metal, and the degrees of

* **收稿日期：**　2021-10-26; **修订日期：**　2022-03-19
基金项目：　国家自然科学基金(11802101; 11772138)
作者简介：　雷剑(1988—)，男，讲师，博士(E-mail: swordlei@hust.edu.cn)；
何玉明(1962—)，男，教授，博士(通讯作者. E-mail: ymhe@hust.edu.cn).
引用格式：　雷剑，谢宇阳，姚明格，何玉明. 变截面二维功能梯度微梁的振动和屈曲特性[J]. 应用数学和力学，2022，**43**(10)：1133-1145.

increase are different under different boundary conditions. The thick-direction and axial material gradient indexes also have significant influences on the free vibration and buckling behavior of the microbeam.

Key words: modified couple stress theory; functionally graded material; variable-cross-section beam; size effect; vibration and buckling

引 言

功能梯度结构是近三十年发展起来的一种新型复合结构,其是由两种以上材料依据特定的设计原则,所形成的材料性能沿一定方向光滑变化的组织和结构.相比传统复合结构,功能梯度结构的显著特点是各组分间没有明显的界面,避免了因材料性能突变而造成的应力集中和层间破坏.目前,功能梯度材料在工程中得到了广泛应用,如土木工程、船舶和航空航天工程等.

建立功能梯度结构力学行为的理论模型并分析其内在规律是功能梯度结构的优化设计和工程应用的前提和基础.基于此,国内外诸多学者开展了相关研究工作.例如,Sina 等[1] 建立了功能梯度梁自由振动的解析模型并分析了边界条件、体积分数等对固有频率和模态的影响.Alshorbagy 等[2] 基于 Euler-Bernoulli 梁理论和虚功原理建立了功能梯度梁的自由振动力学模型,并用有限元法得到了相关数值解.Şimşek[3] 研究了移动质量块影响下功能梯度梁的振动特性.Aydogdu[4] 采用半逆解法分析了轴向功能梯度梁的振动和屈曲行为.王伟斌等[5] 建立了多孔功能梯度材料 Timoshenko 梁的力学模型,并分析了其自由振动特性.蒲育等[6] 基于改进型广义微分求积法研究了功能梯度梁的屈曲行为.马连生等[7] 应用一阶剪切变形理论研究了 FGM 梁的过屈曲行为.此外,葛仁余等[8] 基于 Euler-Bernoulli 梁理论,研究了轴向载荷下轴向功能梯度变截面梁的振动和屈曲问题.杜运兴等[9] 基于物理中面的概念,研究了轴向力作用下材料性能沿厚度方向变化的变截面功能梯度 Timoshenko 梁的振动特性.

随着材料科学、微电子技术和微加工技术的发展,各类微/纳米机电系统 (MEMS/NEMS) 相继出现并得到广泛应用,功能梯度结构的应用范围也被进一步拓展到了 MEMS/NEMS 领域[10-11].微纳米结构的一个显著特点是其力学行为表现出明显的尺度效应[12-15].为描述微结构力学行为的尺度效应,包含额外材料尺度参数的非经典连续介质力学理论相继出现并得到了广泛的应用,如非局部弹性理论[16]、应变梯度弹性理论[13] 和修正的偶应力理论[17] 等.

近些年来,许多研究者针对微尺度功能梯度梁结构的力学性能开展了研究工作.Asghari 等[18] 基于 Euler-Bernoulli 梁理论和修正的偶应力理论分析了功能梯度微尺度梁的静态弯曲和自由振动尺度效应.Reddy[19] 基于 Euler-Bernoulli 和 Timoshenko 梁理论建立了功能梯度微尺度梁静态弯曲、自由振动和屈曲力学模型,并分析了尺度参数、材料梯度指数等的影响.随后,Şimşek 和 Reddy[20] 基于统一的高阶剪切变形梁理论和修正的偶应力理论研究了功能梯度微尺度梁的弯曲和振动行为.考虑物理中面的影响,Al-Basyouni 和 Tounsi 等[21] 研究了功能梯度微尺度梁的弯曲和动态特性.Lei 等[22] 基于应变梯度弹性理论和正弦剪切变形梁理论对功能梯度微梁的静动态力学特性和稳定性问题进行了研究.此外,Lei 等基于修正的偶应力理论和非局部热弹性理论分别研究了热环境下微米量级功能梯度梁的振动和屈曲特性[23] 以及轴向功能梯度纳米梁的热屈曲行为[24].杨子豪等[25] 基于新修正偶应力理论研究了平面正交各向异性功能梯度微梁的自由振动行为.Ebrahimi 等[26] 建立了剪切变形功能梯度纳米曲梁的屈曲模型,模型中同时考虑了非局部效应和应变梯度效应的影响.

以上研究工作主要针对宏微观厚度方向和轴向功能梯度梁的力学性能开展,其材料性能沿一个方向连续变化.目前,材料性能沿单方向变化的一维功能梯度结构已无法完全满足工程结构在不同方向上的温度和应力分布要求,开展材料性能同时沿厚度和轴向变化的二维功能梯度结构力学性能的研究工作显得更为迫切和重要.例如,Lei 等[27] 基于一新颖的高阶剪切变形理论研究了二维功能梯度梁的后屈曲行为,并分析了孔隙率的影响.Tang 等[28] 研究了湿热环境下二维功能梯度梁的非线性振动特性.Barati 等[29] 分析了磁场中二维功能梯度纳米梁的横向振动行为.Huang 等[30] 研究得到了二维功能梯度 Timoshenko 梁静态弯曲变形的精确解.

本文的主要目的是建立变截面二维功能梯度微尺度梁自由振动和稳定性问题的力学模型,研究梁的锥度

比、功能梯度指数和轴向功能梯度指数、尺度效应等因素对其振动和屈曲行为的影响, 以期为多维功能梯度结构的设计和优化提供理论支撑.

1　理论模型

1.1　变截面二维功能梯度微尺度梁

考虑如图 1 所示的微尺度变截面二维功能梯度梁, 长度为 L, 厚度和宽度随坐标 x 变化, 分别记为$h(x)$和$b(x)$, 其材料性能同时沿厚度方向和轴向连续变化. 假定组分材料的体积分数符合幂律分布, 根据混合律模型[31-32], 微梁的等效材料性能可以表示为

$$\Gamma(x,z)=(\Gamma_{\mathrm{c}}-\Gamma_{\mathrm{m}})\left(\frac{1}{2}+\frac{z}{h(x)}\right)^{P_z}\left(\frac{x}{L}\right)^{P_x}+\Gamma_{\mathrm{m}}, \tag{1}$$

式中, P_x和P_z为非负参数, 分别表示轴向功能梯度指数和厚度方向功能梯度指数. 下标“c”和“m”分别表示材料的陶瓷组分和金属组分. 当 Γ 分别为 E, ν和ρ时, 可以得到微梁的等效弹性模量、等效 Poisson 比和等效密度.

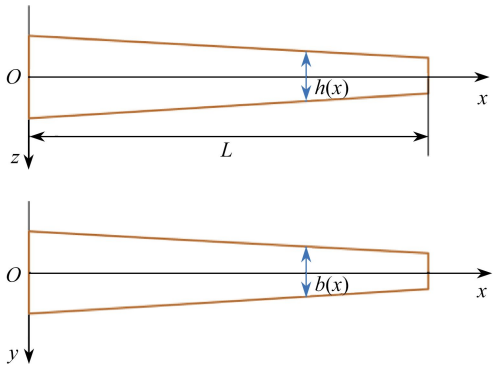

图 1　二维变截面功能梯度微梁示意图

Fig. 1　Schematic diagram of a 2D variable-cross-section functionally graded microbeam

设定梁的厚度和宽度沿轴向线性变化, 有

$$h(x)=h_{\mathrm{L}}\left(1-c_h\frac{x}{L}\right), \tag{2}$$

$$b(x)=b_{\mathrm{L}}\left(1-c_b\frac{x}{L}\right), \tag{3}$$

式中, h_{L}和b_{L}分别为微梁左端面的厚度和宽度, c_h和c_b($0\leqslant c_h<1$, $0\leqslant c_b<1$)分别为微梁对应于厚度和宽度的锥度比.

1.2　振动和屈曲行为的控制方程

采用图 1 中的直角坐标系, 基于 Timoshenko 梁理论, 二维功能梯度变截面微尺度梁上任意一点的位移为

$$\begin{cases}u_x(x,z,t)=u(x,t)+z\phi(x,t),\\ u_y(x,z,t)=0,\\ u_z(x,z,t)=w(x,t),\end{cases} \tag{4}$$

式中, u 和 w 分别为微梁几何中面上一点的轴向和横向位移, ϕ 为微梁横截面绕 y 轴的转角.

传统应变张量的非零分量为

$$\varepsilon_{xx}=\frac{\partial u}{\partial x}+z\frac{\partial\phi}{\partial x},\ \varepsilon_{xz}=\frac{1}{2}\left(\phi+\frac{\partial w}{\partial x}\right). \tag{5}$$

根据 Hooke 定律, 可得微梁的轴向正应力和横向剪应力为

$$\sigma_{xx}=E(x,z)\left(\frac{\partial u}{\partial x}+z\frac{\partial\phi}{\partial x}\right),\ \sigma_{xz}=k_{\mathrm{s}}\mu(x,z)\left(\phi+\frac{\partial w}{\partial x}\right), \tag{6}$$

式中, k_s为剪切修正系数.

Yang 等[17] 发展的修正的偶应力理论含有一个与材料微结构有关的内禀特征尺度参数, 可以预测微尺度构件力学行为的尺度效应. 其本构关系中对称曲率张量χ_{ij}和偶应力张量的偏斜部分m_{ij}分别定义如下:

$$\chi_{ij}=\frac{1}{2}(e_{ipq}\partial_p\varepsilon_{qj}+e_{jpq}\partial_p\varepsilon_{qi}), \tag{7}$$

$$m_{ij}=2\mu l^2\chi_{ij}, \tag{8}$$

式中, l 为材料内禀特征尺度参数, μ为剪切模量.

材料内禀特征尺度参数是微尺度材料的本征材料常数, 已有研究者通过静态弯曲实验得出环氧树脂(epoxy)的尺度参数为 17.6 μm[13]. 对于金属材料, 已通过振动实验测得镍(Ni)、铜(Cu)和钛(Ti)的尺度参数分别为 1.553 μm, 1.422 μm 和 0.775 μm[14-15]. 从以上研究中可以看出, 不同材料的内禀特征尺度参数是有差异的, 尤其是不同种类的材料. 因此, 对于由金属和陶瓷组成的二维功能梯度微尺度梁, 根据以上分析, 并参考文献 [21, 33], 我们假定其内禀特征尺度参数同样符合混合律. 根据式(1), 微梁的等效材料内秉特征尺度参数可以表示为

$$l(x,z)=(l_{\mathrm{c}}-l_{\mathrm{m}})\left(\frac{1}{2}+\frac{z}{h(x)}\right)^{P_z}\left(\frac{x}{L}\right)^{P_x}+l_{\mathrm{m}}, \tag{9}$$

式中, l_{c}和l_{m}分别为陶瓷和金属材料的内禀特征尺度参数.

将式(5)代入式(7)中, 可得对称旋转梯度张量的非零分量为

$$\chi_{xy}=\frac{1}{4}\left(\frac{\partial\phi}{\partial x}-\frac{\partial^2 w}{\partial x^2}\right). \tag{10}$$

将式(10)代入式(8)中, 可得偶应力张量的非零分量为

$$m_{xy}=\frac{1}{2}l^2(x,z)\mu(x,z)\left(\frac{\partial\phi}{\partial x}-\frac{\partial^2 w}{\partial x^2}\right). \tag{11}$$

微梁在时间区间 $[t_1, t_2]$ 上累积的应变能的一阶变分表达式为

$$\begin{aligned}\delta\int_{t_1}^{t_2}U\mathrm{d}t=&\int_{t_1}^{t_2}\left[\int_{\Omega}(\sigma_{xx}\delta\varepsilon_{xx}+2\sigma_{xz}\delta\varepsilon_{xz}+2m_{xy}\delta\chi_{xy})\mathrm{d}\Omega\right]\mathrm{d}t=\\&\int_{t_1}^{t_2}\left[\int_x\left(-\frac{\partial N}{\partial x}\delta u-\frac{\partial Q}{\partial x}\delta w-\frac{1}{2}\frac{\partial^2 P}{\partial x^2}\delta w-\frac{\partial M}{\partial x}\delta\phi+Q\delta\phi-\frac{1}{2}\frac{\partial P}{\partial x}\delta\phi\right)\mathrm{d}x\right]\mathrm{d}t+\\&\int_{t_1}^{t_2}\left(N\delta u+Q\delta w+\frac{1}{2}\frac{\partial P}{\partial x}\delta w-\frac{1}{2}P\frac{\partial\delta w}{\partial x}+M\delta\phi+\frac{1}{2}P\delta\phi\right)\Bigg|_{x=0}^{x=L}\mathrm{d}t,\end{aligned} \tag{12}$$

式中, N, M, P 和 Q 为各应力分量在微梁横截面上的合力, 其表达式分别为

$$N=\int_A\sigma_{xx}\mathrm{d}A,\ M=\int_A z\sigma_{xx}\mathrm{d}A,\ P=\int_A m_{xy}\mathrm{d}A,\ Q=\int_A\sigma_{xz}\mathrm{d}A, \tag{13}$$

其中, A 为微梁的横截面积, 其大小为坐标 x 的函数,

$$A(x)=h_{\mathrm{L}}b_{\mathrm{L}}\left(1-c_h\frac{x}{L}\right)\left(1-c_b\frac{x}{L}\right). \tag{14}$$

微梁在时间区间 $[t_1, t_2]$ 上累积的动能的一阶变分表达式为

$$\begin{aligned}\delta\int_{t_1}^{t_2}K\mathrm{d}t=&\int_{t_1}^{t_2}\int_{\Omega}\rho(x,z)\left(\frac{\partial u_x}{\partial t}\frac{\partial\delta u_x}{\partial t}+\frac{\partial u_y}{\partial t}\frac{\partial\delta u_y}{\partial t}+\frac{\partial u_z}{\partial t}\frac{\partial\delta u_z}{\partial t}\right)\mathrm{d}\Omega\mathrm{d}t=\\&\int_{t_1}^{t_2}\int_0^L\left[\left(-m_0\frac{\partial^2 u}{\partial t^2}-m_1\frac{\partial^2\phi}{\partial t^2}\right)\delta u+\left(-m_1\frac{\partial^2 u}{\partial t^2}-m_2\frac{\partial^2\phi}{\partial t^2}\right)\delta\phi-m_0\frac{\partial^2 w}{\partial t^2}\delta w\right]\mathrm{d}x\mathrm{d}t,\end{aligned} \tag{15}$$

式中

$$(m_0,\ m_1,\ m_2)=\int_A\rho(x,z)(1,\ z,\ z^2)\mathrm{d}A. \tag{16}$$

轴向载荷 N_x 在时间区间 $[t_1, t_2]$ 上所做的功的一阶变分为

$$\delta\int_{t_1}^{t_2} W\mathrm{d}t = \int_{t_1}^{t_2}\int N_x\frac{\partial w}{\partial x}\frac{\partial\delta w}{\partial x}\mathrm{d}x\mathrm{d}t = -\int_{t_1}^{t_2}\int_0^L N_x\frac{\partial^2 w}{\partial x^2}\delta w\mathrm{d}x\mathrm{d}t + \int_{t_1}^{t_2} N_x\frac{\partial w}{\partial x}\delta w\Big|_0^L\mathrm{d}t. \tag{17}$$

微梁振动和屈曲行为的控制方程可由 Hamilton 变分原理获得:

$$\delta\int_{t_1}^{t_2}[(U-W)-K]\mathrm{d}t = 0. \tag{18}$$

将式(12)、(15)和(17)代入式(18)中, 可得微梁的运动方程为

$$\delta u:\ -\frac{\partial N}{\partial x} + m_0\frac{\partial^2 u}{\partial t^2} + m_1\frac{\partial^2\phi}{\partial t^2} = 0, \tag{19}$$

$$\delta w:\ -\frac{\partial Q}{\partial x} - \frac{1}{2}\frac{\partial^2 P}{\partial x^2} + N_x\frac{\partial^2 w}{\partial x^2} + m_0\frac{\partial^2 w}{\partial t^2} = 0, \tag{20}$$

$$\delta\phi:\ -\frac{\partial M}{\partial x} + Q - \frac{1}{2}\frac{\partial P}{\partial x} + m_1\frac{\partial^2 u}{\partial t^2} + m_2\frac{\partial^2\phi}{\partial t^2} = 0. \tag{21}$$

微梁两端部($x=0$和$x=L$)的边界条件为

$$u = 0 \quad \text{or} \quad N = 0, \tag{22}$$

$$w = 0 \quad \text{or} \quad Q + \frac{1}{2}\frac{\partial P}{\partial x} - N_x\frac{\partial w}{\partial x} = 0, \tag{23}$$

$$\frac{\partial w}{\partial x} = 0 \quad \text{or} \quad P = 0, \tag{24}$$

$$\phi = 0 \quad \text{or} \quad M + \frac{1}{2}P = 0, \tag{25}$$

其中, 端部为固支边界时, 应满足$u=0$, $w=0$, $\dfrac{\partial w}{\partial x}=0$和$\phi=0$; 端部为铰支边界时, 应满足$u=0$和$w=0$; 端部为自由边界时, 对端部的位移没有限制.

将式(13)代入式(19)~(21)中, 可得微梁位移形式的运动方程为

$$\delta u:\ -\frac{\partial}{\partial x}\left(A_{xx}\frac{\partial u}{\partial x}\right) - \frac{\partial}{\partial x}\left(B_{xx}\frac{\partial\phi}{\partial x}\right) + m_0\frac{\partial^2 u}{\partial t^2} + m_1\frac{\partial^2\phi}{\partial t^2} = 0, \tag{26}$$

$$\delta w:\ -\frac{\partial}{\partial x}(C_{xz}\phi) - \frac{\partial}{\partial x}\left(C_{xz}\frac{\partial w}{\partial x}\right) - \frac{1}{4}\frac{\partial^2}{\partial x^2}\left(C_{xy}\frac{\partial\phi}{\partial x}\right) + \frac{1}{4}\frac{\partial^2}{\partial x^2}\left(C_{xy}\frac{\partial^2 w}{\partial x^2}\right) + N_x\frac{\partial^2 w}{\partial x^2} + m_0\frac{\partial^2 w}{\partial t^2} = 0, \tag{27}$$

$$\delta\phi:\ -\frac{\partial}{\partial x}\left(B_{xx}\frac{\partial u}{\partial x}\right) - \frac{\partial}{\partial x}\left(D_{xx}\frac{\partial\phi}{\partial x}\right) + C_{xz}\phi + C_{xz}\frac{\partial w}{\partial x} - \frac{1}{4}\frac{\partial}{\partial x}\left(C_{xy}\frac{\partial\phi}{\partial x}\right) + \frac{1}{4}\frac{\partial}{\partial x}\left(C_{xy}\frac{\partial^2 w}{\partial x^2}\right) + m_1\frac{\partial^2 u}{\partial t^2} + m_2\frac{\partial^2\phi}{\partial t^2} = 0, \tag{28}$$

式中

$$(A_{xx},\ B_{xx},\ D_{xx}) = \int_A (1,\ z,\ z^2)E(x,z)\mathrm{d}A, \tag{29}$$

$$C_{xy} = \int_A l^2(x,z)\mu(x,z)\mathrm{d}A,$$

$$C_{xz} = k_{\mathrm{s}}\int_A \mu(x,z)\mathrm{d}A. \tag{30}$$

同样地, 微梁两端部($x=0$和$x=L$)位移形式的边界条件为

$$u = 0 \quad \text{or} \quad A_{xx}\frac{\partial u}{\partial x} + B_{xx}\frac{\partial\phi}{\partial x} = 0, \tag{31}$$

$$w = 0 \quad \text{or} \quad C_{xz}\phi + C_{xz}\frac{\partial w}{\partial x} + \frac{1}{4}\frac{\partial}{\partial x}\left(C_{xy}\frac{\partial\phi}{\partial x}\right) - \frac{1}{4}\frac{\partial}{\partial x}\left(C_{xy}\frac{\partial^2 w}{\partial x^2}\right) - N_x\frac{\partial w}{\partial x} = 0, \tag{32}$$

$$\frac{\partial w}{\partial x}=0 \quad \text{or} \quad C_{xy}\frac{\partial \phi}{\partial x}-C_{xy}\frac{\partial^2 w}{\partial x^2}=0, \tag{33}$$

$$\phi=0 \quad \text{or} \quad B_{xx}\frac{\partial u}{\partial x}+D_{xx}\frac{\partial \phi}{\partial x}+\frac{1}{4}C_{xy}\frac{\partial \phi}{\partial x}-\frac{1}{4}C_{xy}\frac{\partial^2 w}{\partial x^2}=0. \tag{34}$$

2 振动和屈曲问题的 Ritz 解法

应用 Ritz 法, 可以获得任意边界条件下变截面二维功能梯度微梁振动和稳定性问题的数值解.

对微梁振动和屈曲控制方程进行加权积分, 可得弱形式的控制方程, 其等效于相应的运动方程和边界条件. 根据式(26)~(28), 变截面二维功能梯度微尺度梁弱形式的控制方程可由以下加权积分得到:

$$\int_0^L -\psi_1\left\{-\frac{\partial}{\partial x}\left(A_{xx}\frac{\partial u}{\partial x}\right)-\frac{\partial}{\partial x}\left(B_{xx}\frac{\partial \phi}{\partial x}\right)+m_0\frac{\partial^2 u}{\partial t^2}+m_1\frac{\partial^2 \phi}{\partial t^2}\right\}\mathrm{d}x=0, \tag{35}$$

$$\int_0^L -\psi_2\left\{-\frac{\partial}{\partial x}(C_{xz}\phi)-\frac{\partial}{\partial x}\left(C_{xz}\frac{\partial w}{\partial x}\right)-\frac{1}{4}\frac{\partial^2}{\partial x^2}\left(C_{xy}\frac{\partial \phi}{\partial x}\right)+\frac{1}{4}\frac{\partial^2}{\partial x^2}\left(C_{xy}\frac{\partial^2 w}{\partial x^2}\right)+N_x\frac{\partial^2 w}{\partial x^2}+m_0\frac{\partial^2 w}{\partial t^2}\right\}\mathrm{d}x=0, \tag{36}$$

$$\begin{aligned}\int_0^L -\psi_3\Bigg\{&-\frac{\partial}{\partial x}\left(B_{xx}\frac{\partial u}{\partial x}\right)-\frac{\partial}{\partial x}\left(D_{xx}\frac{\partial \phi}{\partial x}\right)+C_{xz}\phi+C_{xz}\frac{\partial w}{\partial x}-\frac{1}{4}\frac{\partial}{\partial x}\left(C_{xy}\frac{\partial \phi}{\partial x}\right)+\\&\frac{1}{4}\frac{\partial}{\partial x}\left(C_{xy}\frac{\partial^2 w}{\partial x^2}\right)+m_1\frac{\partial^2 u}{\partial t^2}+m_2\frac{\partial^2 \phi}{\partial t^2}\Bigg\}\mathrm{d}x=0,\end{aligned} \tag{37}$$

式中, ψ_1, ψ_2和ψ_3为权函数, 分别满足 u, w 和 ϕ 在端部的边界条件.

对式(35)~(37)进行分部积分, 则变截面二维功能梯度微尺度梁弱形式的控制方程为

$$\int_0^L\left\{-\frac{\partial \psi_1}{\partial x}\left(A_{xx}\frac{\partial u}{\partial x}\right)-\frac{\partial \psi_1}{\partial x}\left(B_{xx}\frac{\partial \phi}{\partial x}\right)-\psi_1 m_0\frac{\partial^2 u}{\partial t^2}-\psi_1 m_1\frac{\partial^2 \phi}{\partial t^2}\right\}\mathrm{d}x+\psi_1\left(A_{xx}\frac{\partial u}{\partial x}+B_{xx}\frac{\partial \phi}{\partial x}\right)\Bigg|_0^L=0, \tag{38}$$

$$\begin{aligned}\int_0^L\Bigg\{&-\frac{\partial \psi_2}{\partial x}(C_{xz}\phi)-\frac{\partial \psi_2}{\partial x}\left(C_{xz}\frac{\partial w}{\partial x}\right)+\frac{1}{4}\frac{\partial^2 \psi_2}{\partial x^2}\left(C_{xy}\frac{\partial \phi}{\partial x}\right)-\frac{1}{4}\frac{\partial^2 \psi_2}{\partial x^2}\left(C_{xy}\frac{\partial^2 w}{\partial x^2}\right)+\\&N_x\frac{\partial \psi_2}{\partial x}\frac{\partial w}{\partial x}-\psi_2 m_0\frac{\partial^2 w}{\partial t^2}\Bigg\}\mathrm{d}x+\psi_2\Bigg\{(C_{xz}\phi)+\left(C_{xz}\frac{\partial w}{\partial x}\right)+\frac{1}{4}\frac{\partial}{\partial x}\left(C_{xy}\frac{\partial \phi}{\partial x}\right)-\\&\frac{1}{4}\frac{\partial}{\partial x}\left(C_{xy}\frac{\partial^2 w}{\partial x^2}\right)-N_x\frac{\partial w}{\partial x}\Bigg\}\Bigg|_0^L-\frac{1}{4}\frac{\partial \psi_2}{\partial x}\left(C_{xy}\frac{\partial \phi}{\partial x}-C_{xy}\frac{\partial^2 w}{\partial x^2}\right)\Bigg|_0^L=0,\end{aligned} \tag{39}$$

$$\begin{aligned}\int_0^L\Bigg\{&-\frac{\partial \psi_3}{\partial x}\left(B_{xx}\frac{\partial u}{\partial x}\right)-\frac{\partial \psi_3}{\partial x}\left(D_{xx}\frac{\partial \phi}{\partial x}\right)-\psi_3 C_{xz}\phi-\psi_3 C_{xz}\frac{\partial w}{\partial x}-\\&\frac{1}{4}\frac{\partial \psi_3}{\partial x}\left(C_{xy}\frac{\partial \phi}{\partial x}\right)+\frac{1}{4}\frac{\partial \psi_3}{\partial x}\left(C_{xy}\frac{\partial^2 w}{\partial x^2}\right)-\psi_3 m_1\frac{\partial^2 u}{\partial t^2}-\psi_3 m_2\frac{\partial^2 \phi}{\partial t^2}\Bigg\}\mathrm{d}x+\\&\psi_3\left(B_{xx}\frac{\partial u}{\partial x}+D_{xx}\frac{\partial \phi}{\partial x}+\frac{1}{4}C_{xy}\frac{\partial \phi}{\partial x}-\frac{1}{4}C_{xy}\frac{\partial^2 w}{\partial x^2}\right)\Bigg|_0^L=0,\end{aligned} \tag{40}$$

式中, 域内积分部分为微梁的运动方程, 边界积分为对应的运动边界条件.

将位移函数u, w和ϕ展开成以下形式:

$$u(x,t)=\tilde{u}(x)\mathrm{e}^{\mathrm{i}\omega t},\ w(x,t)=\tilde{w}(x)\mathrm{e}^{\mathrm{i}\omega t},\ \phi(x,t)=\tilde{\phi}(x)\mathrm{e}^{\mathrm{i}\omega t}. \tag{41}$$

根据 Ritz 法, 将$\tilde{u}$, $\tilde{w}$和$\tilde{\phi}$展开成以下形式:

$$\tilde{u}=f_1(x)\sum_{j=1}^{n_\mathrm{t}}a_j\left(\frac{x}{L}\right)^{j-1},\ \tilde{w}=f_2(x)\sum_{j=1}^{n_\mathrm{t}}b_j\left(\frac{x}{L}\right)^{j-1},\ \tilde{\phi}=f_3(x)\sum_{j=1}^{n_\mathrm{t}}c_j\left(\frac{x}{L}\right)^{j-1}, \tag{42}$$

式中, a_j, b_j和c_j为待定系数; $f_1(x)$, $f_2(x)$和$f_3(x)$为满足边界条件的函数, 定义如下:

$$f_1(x)=x^{p_1}(x-L)^{p_2},\ f_2(x)=x^{s_1}(x-L)^{s_2},\ f_3(x)=x^{t_1}(x-L)^{t_2}, \tag{43}$$

其中, 指标p_1, p_2, s_1, s_2和t_1, t_2用于指定不同类型的边界条件, 根据前述的位移限制条件, 可得各指标的值, 如表 1 所示(表中 C-C 表示两端固支, H-H 表示两端铰结, F-F 表示两端自由; C-H 表示左端固支右端铰结; H-C 表示左端铰结右端固支; C-F 表示左端固支右端自由; F-C 表示左端自由右端固支, 后同).

根据推导弱形式控制方程的相关原理, 可令权函数ψ_1, ψ_2和ψ_3分别等于边界函数$f_1(x)$, $f_2(x)$和$f_3(x)$.

将式(41)代入式(38)~(40)中, 消去时间项, 由控制方程的域内积分部分, 可得到相应的特征值方程, 对特征值方程进行求解, 可得到微梁振动和屈曲问题的数值解. 为了便于对比分析, 引入以下无量纲参数:

$$\bar{\omega}=\frac{\omega L^2}{h_{\mathrm{L}}}\sqrt{\frac{\rho_{\mathrm{m}}}{E_{\mathrm{m}}}},\ \bar{N}_x=\frac{12L^2}{b_{\mathrm{L}}h_{\mathrm{L}}^3E_{\mathrm{m}}}N_x. \tag{44}$$

表 1　不同边界条件时 p_1, p_2, s_1, s_2 及 t_1, t_2 的取值

Table 1　Values of p_1, p_2, s_1, s_2 and t_1, t_2 with different boundary conditions

	p_1	p_2	s_1	s_2	t_1	t_2
C-C	1	1	2	2	1	1
H-H	1	1	1	1	0	0
F-F	0	0	0	0	0	0
C-H	1	1	2	1	1	0
H-C	1	1	1	2	0	1
C-F	1	0	2	0	1	0
F-C	0	1	0	2	0	1

3　算例分析与结果讨论

本节将给出基于 Ritz 法的若干数值算例, 详细分析尺度效应、锥度比、功能梯度指数等对变截面二维功能梯度微梁一阶固有频率和一阶临界屈曲载荷的影响. 为便于表述, 后续提到固有频率和屈曲载荷时均省略“一阶”. 如无特别声明, 设定功能梯度微梁由铝(Al: $E_{\mathrm{m}}=70$ GPa, $\rho_{\mathrm{m}}=2\,702$ kg/m^3, $\nu_{\mathrm{m}}=0.3$)和氧化铝(Al_2O_3: $E_{\mathrm{c}}=380$ GPa, $\rho_{\mathrm{c}}=3\,960$ kg/m^3, $\nu_{\mathrm{c}}=0.3$)组成. 假定微梁左端部的宽度等于左端部的厚度. 此外, 根据 1.2 小节中的分析, 金属组分 Al 的内禀特征尺度参数取为$l_{\mathrm{m}}=1.5$ μm, 因文献中没有关于陶瓷材料内禀特征尺度参数的相关实验数据, 不妨设定陶瓷组分 Al_2O_3 的内禀特征尺度参数等于金属组分的内禀特征尺度参数($l_{\mathrm{c}}=l_{\mathrm{m}}=1.5$ μm).

3.1　结果验证

为验证当前力学模型的收敛性, 表 2 给出了n_{t}逐渐增大时两端固支等截面二维功能梯度微梁的无量纲频率. 从表中结果可以看出, 随着n_{t}的增加, 计算结果迅速收敛, 当n_{t}取 14 时, 所得结果满足精度要求. 此外, 表 3 给出了宏观功能梯度等截面梁无量纲频率本文模型的计算结果与文献 [34] 中结果的对比, 从中可以看出, 两者吻合较好. 表 4 给出了宏观均质锥形梁无量纲频率本文模型的计算结果与文献 [35] 中基于 Euler-Bernoulli 梁理论的结果对比, 两者相吻合. 以上分析表明, 本文模型是准确可靠的.

表 2　二维功能梯度等截面微梁无量纲频率的收敛性分析($h_{\mathrm{L}}=1.5$ μm, $L=20h_{\mathrm{L}}$, $c_h=c_b=0$, $l_{\mathrm{c}}=l_{\mathrm{m}}=1.5$ μm)

Table 2　Convergence analysis of dimensionless frequencies of the 2D functionally graded equal-cross-section microbeam ($h_{\mathrm{L}}=1.5$ μm, $L=20h_{\mathrm{L}}$, $c_h=c_b=0$, $l_{\mathrm{c}}=l_{\mathrm{m}}=1.5$ μm)

n_{t}	$P_x=P_z=0$	$P_x=0$, $P_z=1$	$P_x=1$, $P_z=0$	$P_x=P_z=1$
6	28.594 0	23.691 1	22.449 8	19.561 0
8	28.583 8	23.682 9	22.436 3	19.552 1
10	28.579 9	23.679 5	22.430 7	19.548 4
12	28.578 5	23.678 3	22.428 6	19.547 1
14	28.578 1	23.677 9	22.427 9	19.546 6
16	28.578 0	23.677 8	22.427 7	19.546 5
18	28.577 9	23.677 7	22.427 6	19.546 4

表 3 基于本文模型的宏观功能梯度等截面梁无量纲频率与文献 [34] 中结果的对比（$h = 1$ m）

Table 3 Comparison of dimensionless frequencies of macro traditional equal-cross-section FG beams with ref.[34] ($h = 1$ m)

BC	L/h	model	P_z				
			0	1	2	5	10
C-F	5	present	1.89472	1.46296	1.33372	1.26441	1.22393
		ref. [34]	1.89479	1.46300	1.33376	1.26445	1.22398
	20	present	1.94957	1.50104	1.36968	1.30374	1.26494
		ref. [34]	1.94957	1.50104	1.36968	1.30375	1.26495
C-C	5	present	10.0198	7.91520	7.20210	6.65777	6.33031
		ref. [34]	10.0344	7.92529	7.21134	6.66764	6.34062
	20	present	12.2226	9.43080	8.60350	8.16921	7.91202
		ref. [34]	12.2235	9.43135	8.60401	8.16985	7.91275

表 4 基于本文模型的宏观均质锥形梁前三阶无量纲频率与文献 [35] 中结果的对比（C-F 边界，$P_z = P_x = 0$，此算例中$\tilde{\omega} = \omega L^2\sqrt{\rho_c A_L/(E_c I_L)}$，$A_L = h_L b_L$，$I_L = b_L h_L^3/12$）

Table 4 Comparison of the 1st 3 order dimensionless frequencies of macro traditional tapered beams with ref.[35] (in this case：C-F boundary condition，$P_z = P_x = 0$，$\tilde{\omega} = \omega L^2\sqrt{\rho_c A_L/(E_c I_L)}$，$A_L = h_L b_L$，$I_L = b_L h_L^3/12$)

c_b	model	c_h=0			c_h	model	c_b=0		
		$\tilde{\omega}_1$	$\tilde{\omega}_2$	$\tilde{\omega}_3$			$\tilde{\omega}_1$	$\tilde{\omega}_2$	$\tilde{\omega}_3$
0	present	3.5090	21.7373	59.7804	0	present	3.5090	21.7373	59.7804
	ref. [35]	3.5160	22.0345	61.6972		ref. [35]	3.5160	22.0345	61.6972
0.4	present	4.0879	22.8068	60.8214	0.4	present	3.7307	18.9405	49.3059
	ref. [35]	4.0970	23.1186	62.7763		ref. [35]	3.7371	19.1138	50.3537
0.8	present	5.3829	25.2969	63.6608	0.8	present	4.2863	15.6622	36.4756
	ref. [35]	5.3976	25.6558	65.7470		ref. [35]	4.2925	15.7427	36.8855

3.2 算例分析

图 2~5 给出了不同边界条件下，微梁的无量纲频率随锥度比变化的情况．从图 2 中可以看出，对于两端固支锥形微梁，无量纲频率随着锥度比c_h的增大逐渐减小；对于锥度比c_b，当其较小时（$0 \leqslant c_b \leqslant 0.6$），无量纲频率变化不明显，当$c_b$继续增大时，无量纲频率有较为明显的减小．在图 3 中，两端铰支锥形微梁的无量纲频率随锥度比变化情况与两端固支时类似．从图 4 可以看出，对于两端自由微梁，当锥度比c_h增大时，无量纲频率先减小后增大；当锥度比c_b增大时，无量纲频率在c_b较小时缓慢增加，随后增长较快，这与两端固支和两端铰支边界时有明显差异．

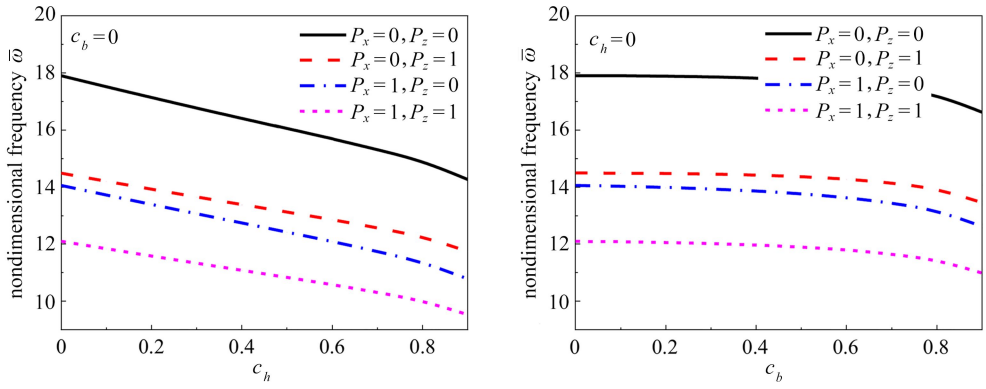

图 2 两端固支边界时锥度比对微梁无量纲频率的影响（$h_L = 3$ μm，$L = 20h_L$，$l_c = l_m = 1.5$ μm）

Fig. 2 The effects of taper ratios on the dimensionless frequencies of microbeams with clamped boundary conditions ($h_L = 3$ μm, $L = 20h_L$, $l_c = l_m = 1.5$ μm)

图 5 展示了左端固支右端自由（C-F）和左端自由右端固支（F-C）边界时锥形微梁的无量纲频率变化情况．结果表明，对于左端固支右端自由（C-F）微梁，其无量纲频率随着锥度比c_h或c_b的增大而增大；相反，对于左

端自由右端固支(F-C)微梁, 其无量纲频率随着锥度比c_h或c_b的增大而减小. 这说明, 对于悬臂边界锥形微梁, 固定端在锥顶(F-C)还是在锥底(C-F)对微梁无量纲频率有重要影响.

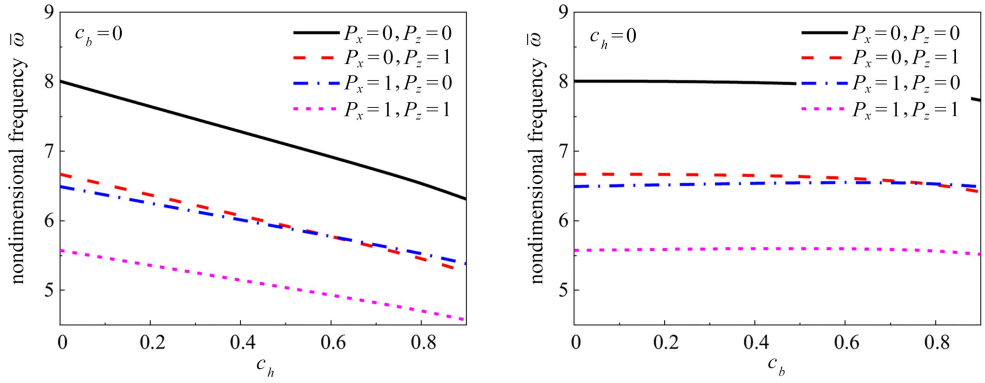

图 3　两端铰支边界时锥度比对微梁无量纲频率的影响(h_L = 3 μm, $L = 20h_L$, $l_c = l_m$ = 1.5 μm)

Fig. 3　The effects of taper ratios on the dimensionless frequencies of microbeams with hinged boundary conditions (h_L = 3 μm, $L = 20h_L$, $l_c = l_m$ = 1.5 μm)

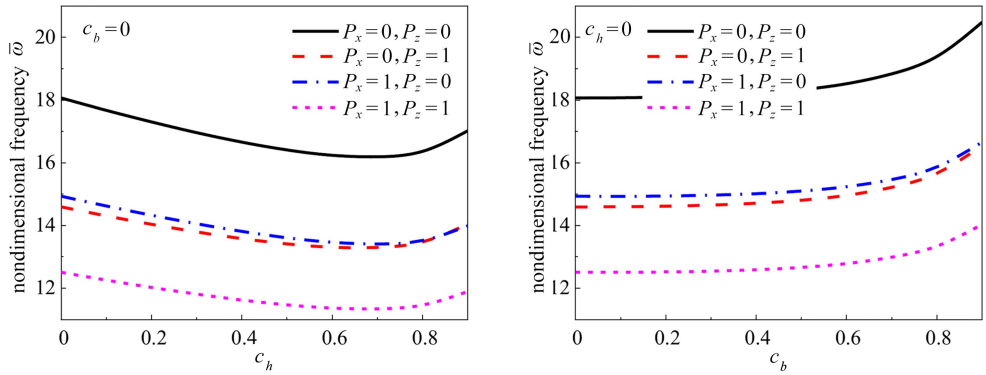

图 4　两端自由边界时锥度比对微梁无量纲频率的影响(h_L = 3 μm, $L = 20h_L$, $l_c = l_m$ = 1.5 μm)

Fig. 4　The effects of taper ratios on the dimensionless frequencies of microbeams with free boundary conditions (h_L = 3 μm, $L = 20h_L$, $l_c = l_m$ = 1.5 μm)

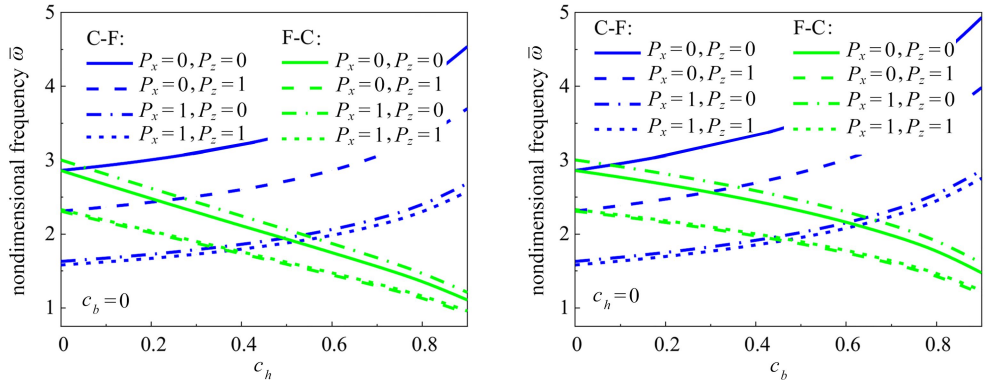

图 5　悬臂边界时锥度比对微梁无量纲频率的影响(h_L = 3 μm, $L = 20h_L$, $l_c = l_m$ = 1.5 μm)

Fig. 5　The effects of taper ratios on the dimensionless frequencies of microbeams with cantilever boundary conditions (h_L = 3 μm, $L = 20h_L$, $l_c = l_m$ = 1.5 μm)

为探究微梁组分材料的轴向梯度分布和微梁轴向变截面效应对其无量纲频率的影响异同, 图 6~8 分别给出了仅考虑材料轴向梯度分布、厚度方向锥度比(c_h)和宽度方向锥度比(c_b)时, 微梁的无量纲频率变化情况. 从图 6 可以看出, 当轴向功能梯度指数较小时(P_x< 5), 微梁无量纲频率随着 P_x 的增大迅速降低, 随后趋于平缓, 这是因为, 轴向功能梯度指数在 0~5 范围内变化时, 微梁轴向的材料分布改变明显, 对微梁频率的影响显著. 从图 7 和图 8 中可以看出, 锥度比(c_h, c_b)对微梁频率的影响与微梁的边界条件相关, 相关影响规律在图 2~5 中已进行了详细描述. 此外, 厚度方向锥度比(c_h)的影响还与微梁的尺度效应相关, 从图 7 中可知, 当考虑微梁的尺度效应时, c_h对微梁无量纲频率的影响减弱. 综合以上分析可知, 三个因素均对微梁的无量纲频率

有显著影响，而影响效果则存在较大差异，微梁的无量纲频率变化规律是微梁的材料分布、变截面效应、尺度效应和边界条件等因素综合作用的结果.

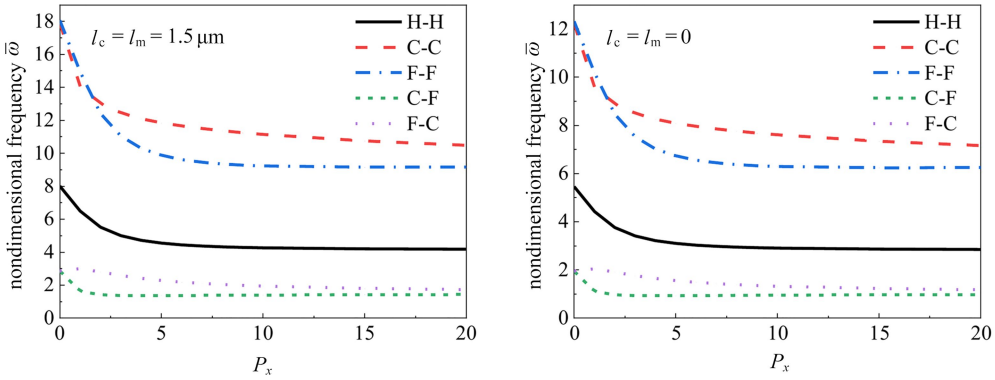

图 6 轴向功能梯度指数对微梁无量纲频率的影响($h_L = 3\ \mu m, L = 20h_L, c_h = c_b = 0, P_z = 0$)

Fig. 6 The effects of axial functional gradient indexes on the dimensional frequencies of microbeams ($h_L = 3\ \mu m, L = 20h_L, c_h = c_b = 0, P_z = 0$)

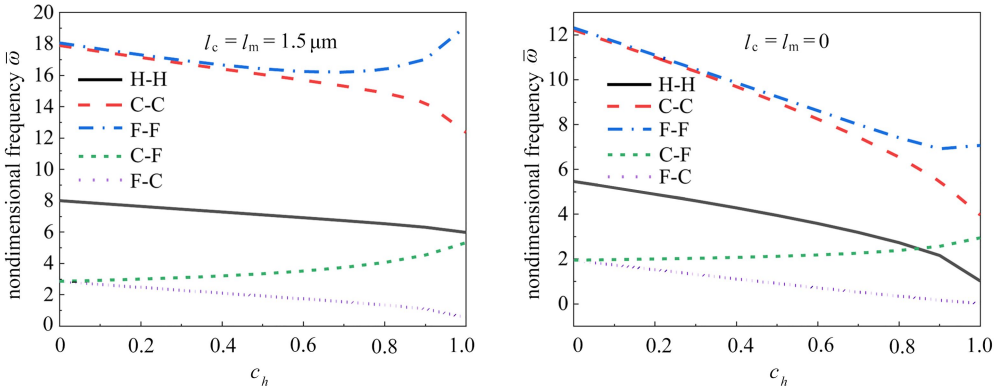

图 7 锥度比(c_h)对微梁无量纲频率的影响($h_L = 3\ \mu m, L = 20h_L, c_b = 0, P_x = P_z = 0$)

Fig. 7 The effects of taper ratios(c_h) on the dimensional frequencies of microbeams ($h_L = 3\ \mu m, L = 20h_L, c_b = 0, P_x = P_z = 0$)

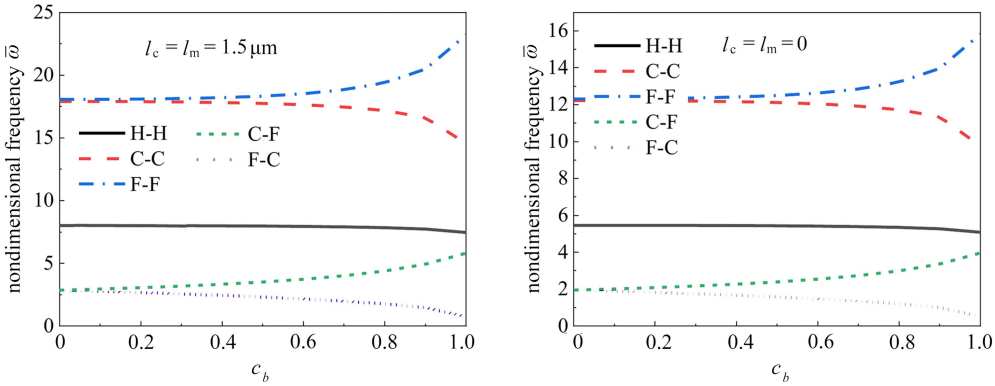

图 8 锥度比(c_b)对微梁无量纲频率的影响($h_L = 3\ \mu m, L = 20h_L, c_h = 0, P_x = P_z = 0$)

Fig. 8 The effects of taper ratios(c_b)on the dimensional frequencies of microbeams ($h_L = 3\ \mu m, L = 20h_L, c_h = 0, P_x = P_z = 0$)

前述分析表明，自由边界时，频率随厚度方向锥度比(c_h)变化时存在极小值点，这与其他边界条件时单调变化不同(图 4 和图 7).为深入探究自由边界时微梁频率随锥度比(c_h)的变化规律，图 9 给出了自由边界时有无尺度效应、不同功能梯度指数下的频率变化情况.图中结果表明不论是否考虑尺度效应，频率随着c_h的变化均出现极小值点，区别在于不考虑尺度效应时，极小值点出现在锥度比很大时(约 0.95)，考虑尺度效应时极小值点位置的c_h约为 0.7.此外，图中结果还说明，功能梯度指数的变化对极值点位置没有明显的影响.综合以上分析可知，频率极值点存在与否与梁是否有外界约束相关，尺度效应则会改变自由边界下频率极值点出现的锥度比(c_h).

图 10 绘制了不同厚度下微梁的无量纲频率随梁的长厚比变化的曲线.结果表明，当微梁为厚梁时($L/h < 10$)，其无量纲频率随着长厚比减小而逐渐减小，当微梁长厚比大于 10 时，微梁的无量纲频率变化趋于

平缓.这说明当梁的长厚比较小时, 剪切变形效应明显, 梁的无量纲刚度明显降低, 无量纲频率降低.此外, 当微梁厚度逐渐增大时, 无量纲频率减小, 说明随着厚度的增加, 小尺度效应逐渐降低.图 11 绘制了陶瓷-金属的内禀特征尺度参数比变化时, 无量纲频率的变化情况.图中结果表明, 总体上来看, 随着陶瓷-金属的特征尺度参数比逐渐增大, 微梁的无量纲频率随之增大; 但是微梁的边界条件不同时, 各曲线的斜率不同, 表明边界条件不同时, 微梁尺度效应的影响不同.

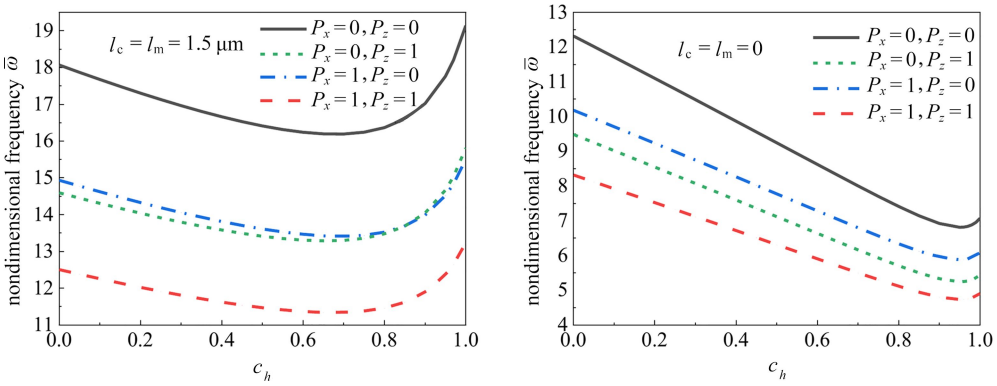

图 9　锥度比(c_h)对自由边界条件微梁无量纲频率的影响($h_L = 3$ μm, $L = 20h_L$, $c_b = 0$, F-F)

Fig. 9　The effects of taper ratios(c_h) on the dimensional frequencies of microbeams with free boundary conditions ($h_L = 3$ μm, $L = 20h_L$, $c_b = 0$, F-F)

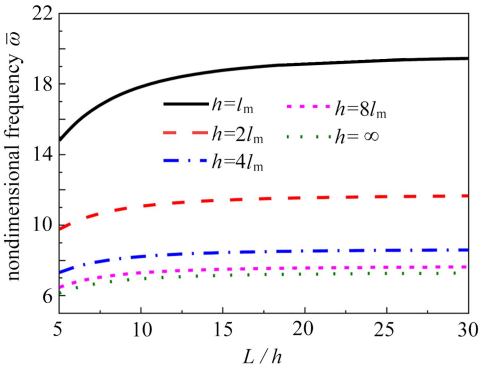

图 10　长厚比对微梁无量纲频率的影响(C-C, $c_h = c_b = 0.2$, $P_x = P_z = 1$, $l_c = l_m = 1.5$ μm)

Fig. 10　The effects of length-to-thickness ratios on the dimensionless frequencies of microbeams (C-C, $c_h = c_b = 0.2$, $P_x = P_z = 1$, $l_c = l_m = 1.5$ μm)

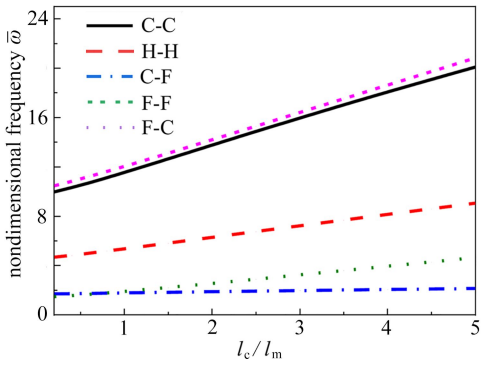

图 11　陶瓷和金属的材料尺度参数比对微梁无量纲频率的影响($h_L = 3$ μm, $L = 20h_L$, $P_x = P_z = 1$, $c_h = c_b = 0.2$, $l_m = 1.5$ μm)

Fig. 11　The effects of the length scale parameter ratios of ceramic and metal on the dimensionless frequencies of microbeams ($h_L = 3$ μm, $L = 20h_L$, $P_x = P_z = 1$, $c_h = c_b = 0.2$, $l_m = 1.5$ μm)

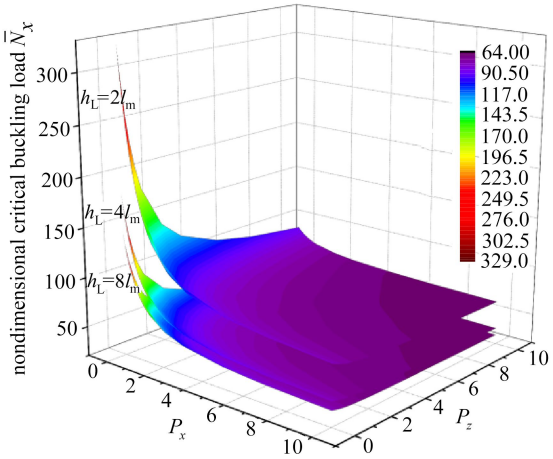

图 12　两端固支(C-C)微梁的临界屈曲载荷随功能梯度指数和轴向功能梯度指数的变化情况($L = 20h_L$, $l_c = l_m = 1.5$ μm, $c_h = c_b = 0.2$)

Fig. 12　The effects of the functionally graded indexes on the critical buckling loads of microbeams ($L = 20h_L$, $l_c = l_m = 1.5$ μm, $c_h = c_b = 0.2$)

图 12 给出了不同厚度下微梁的无量纲临界屈曲载荷随着功能梯度指数和轴向功能梯度指数变化的情

况.结果表明,随着功能梯度指数或轴向功能梯度指数的增大,微梁的无量纲临界屈曲载荷逐渐减小;随着微梁厚度的增大,无量纲临界屈曲载荷同样随之减小.

4 结 论

本文基于修正的偶应力理论和 Timoshenko 梁理论,应用变分原理建立了变截面二维功能梯度微尺度梁自由振动和稳定性问题的力学模型.采用 Ritz 法给出了任意边界下振动基频和临界屈曲载荷的数值解.通过若干数值算例探究了材料内禀特征尺度参数、锥度比、功能梯度指数和轴向功能梯度指数等对微梁振动和屈曲行为的影响,本文主要结论可以总结为:

1) 自由边界时,频率随厚度方向锥度比(c_h)变化时存在极小值点,在其他边界条件下,频率随c_h的改变单调变化.

2) 长厚比较小时,剪切变形效应明显,微梁的无量纲频率降低;微梁厚度逐渐减小时,尺度效应增强,无量纲频率逐渐增加.

3) 微梁的无量纲频率随着陶瓷和金属的材料内禀特征尺度参数比(l_c/l_m)增大而增大,且不同边界条件时,增大的程度不同,这也表明,不同边界条件时,尺度效应对微梁的影响程度不同.

4) 微梁的无量纲临界屈曲载荷随着微梁厚度的增大而减小,随着轴向功能梯度指数或厚度方向功能梯度指数的增大而减小.

参考文献(References):

[1] SINA S, NAVAZI H M, HADDADPOUR H. An analytical method for free vibration analysis of functionally graded beams[J]. *Materials and Design*, 2009, **30**(3): 741-747.

[2] ALSHORBAGY A E, ELTAHER M A, MAHMOUD F. Free vibration characteristics of a functionally graded beam by finite element method[J]. *Applied Mathematical Modelling*, 2011, **35**(1): 412-425.

[3] ŞIMŞEK M. Vibration analysis of a functionally graded beam under a moving mass by using different beam theories[J]. *Composite Structures*, 2010, **92**(4): 904-917.

[4] AYDOGDU M. Semi-inverse method for vibration and buckling of axially functionally graded beams[J]. *Journal of Reinforced Plastics and Composites*, 2008, **27**(7): 683-691.

[5] 王伟斌, 杨文秀, 滕兆春. 多孔功能梯度材料Timoshenko梁的自由振动分析[J]. 计算力学学报, 2021, **5**: 1-13. (WANG Weibin, YANG Wenxiu, TENG Zhaochun. Free vibration analysis of porous functionally graded materials Timoshenko beam[J]. *Chinese Journal of Computational Mechanics*, 2021, **5**: 1-13.(in Chinese))

[6] 蒲育, 周凤玺. FGM梁临界屈曲载荷的改进型GDQ法分析[J]. 应用基础与工程科学学报, 2019, **27**(6): 1308-1320. (PU Yu, ZHOU Fengxi. Critical buckling loads analysis of FGM beams by a modified generalized differential quadrature method[J]. *Journal of Basic Science Engineering*, 2019, **27**(6): 1308-1320.(in Chinese))

[7] 马连生, 贾金政. 机械载荷作用下功能梯度梁的过屈曲分析[J]. 兰州理工大学学报, 2020, **46**(3): 160-164. (MA Liansheng, JIA Jinzheng. Analysis of mechanical postbuckling behavior of functionally graded beams[J]. *Journal of Lanzhou University of Technology*, 2020, **46**(3): 160-164.(in Chinese))

[8] 葛仁余, 张金轮, 韩有民, 等. 功能梯度变截面梁自由振动和稳定性研究[J]. 应用力学学报, 2017, **34**(5): 875-880, 1012. (GE Renyu, ZHANG Jinlun, HAN Youmin, et al. Free vibration and stability of axially functionally graded beams with variable cross-section[J]. *Chinese Journal of Applied Mechanics*, 2017, **34**(5): 875-880, 1012.(in Chinese))

[9] 杜运兴, 程鹏, 周芬. 变截面功能梯度Timoshenko梁的自由振动分析[J]. 湖南大学学报(自然科学版), 2021, **48**(5): 55-62. (DU Yunxing, CHENG Peng, ZHOU Fen. Free vibration analysis of functionally graded Timoshenko beams with variable section[J]. *Journal of Hunan University(Natural Sciences)*, 2021, **48**(5): 55-62.(in Chinese))

[10] LÜ C, LIM C W, CHEN W. Size-dependent elastic behavior of FGM ultra-thin films based on generalized refined theory[J]. *International Journal of Solids and Structures*, 2009, **46**(5): 1176-1185.

[11] SHAAT M, MAHMOUD F, ALSHORBAGY A E, et al. Finite element analysis of functionally graded nano-scale films[J]. *Finite Elements in Analysis and Design*, 2013, **74**: 41-52.

[12] FLECK N A, MULLER G M, ASHBY M F, et al. Strain gradient plasticity: theory and experiment[J]. *Acta Metallurgica et Materialia*, 1994, **42**(2): 475-487.

[13] LAM D C C, MULLER G M, ASHBY M F, et al. Experiments and theory in strain gradient elasticity[J]. *Journal of the Mechanics and Physics of Solids*, 2003, **51**(8): 1477-1508.

[14] LEI J, HE Y, GUO S, et al. Size-dependent vibration of nickel cantilever microbeams: experiment and gradient elasticity[J]. *AIP Advances*, 2016, **6**(10): 105202.

[15] LI Z, HE Y, GUO S, et al. A standard experimental method for determining the material length scale based on modified couple stress theory[J]. *International Journal of Mechanical Sciences*, 2018, **141**: 198-205.

[16] ERINGEN A C, EDELEN D. On nonlocal elasticity[J]. *International Journal of Engineering Science*, 1972, **10**(3): 233-248.

[17] YANG F, CHONG A C M, LAM D C C, et al. Couple stress based strain gradient theory for elasticity[J]. *International Journal of Solids and Structures*, 2002, **39**(10): 2731-2743.

[18] ASGHARI M, CHONG M C, LAM D C C, et al. On the size-dependent behavior of functionally graded micro-beams[J]. *International Journal of Solids and Structure*, 2010, **31**(5): 2324-2329.

[19] REDDY J N. Microstructure-dependent couple stress theories of functionally graded beams[J]. *Journal of the Mechanics and Physics of Solids*, 2011, **59**(11): 2382-2399.

[20] ŞIMŞEK M J, REDDY J N. Bending and vibration of functionally graded microbeams using a new higher order beam theory and the modified couple stress theory[J]. *International Journal of Engineering Science*, 2013, **64**: 37-53.

[21] AL-BASYOUNI K S, TOUNSI A, MAHMOUD S R. Size dependent bending and vibration analysis of functionally graded micro beams based on modified couple stress theory and neutral surface position[J]. *Composite Structures*, 2015, **125**: 621-630.

[22] LEI Jian, HE Yuming, ZHANG Bo, et al. Bending and vibration of functionally graded sinusoidal microbeams based on the strain gradient elasticity theory[J]. *International Journal of Engineering Science*, 2013, **72**: 36-52.

[23] LEI J, HE Y, ZHANG B, et al. Thermal buckling and vibration of functionally graded sinusoidal microbeams incorporating nonlinear temperature distribution using DQM[J]. *Journal of Thermal Stresses*, 2017, **40**(6): 665-689.

[24] LEI J, HR M. Effect of nonlocal thermoelasticity on buckling of axially functionally graded nanobeams[J]. *Journal of Thermal Stresses*, 2019, **42**(4): 526-539.

[25] 杨子豪, 贺丹. 考虑尺度依赖的平面正交各向异性功能梯度微梁的自由振动分析[J]. 复合材料学报, 2017, **34**(10): 2375-2384. (YANG Zihao, HE Dan. Size-dependent free vibration analysis of plane orthotropic functionally graded micro-beams[J]. *Acta Materiae Compositae Sinica*, 2017, **34**(10): 2375-2384.(in Chinese))

[26] EBRAHIMI F, BARATI M R. A nonlocal strain gradient refined beam model for buckling analysis of size-dependent shear-deformable curved FG nanobeams[J]. *Composite Structures*, 2017, **159**: 174-182.

[27] LEI J, GUO S, HE M, et al. Postbuckling analysis of bi-directional functionally graded imperfect beams based on a novel third-order shear deformation theory[J]. *Composite Structures*, 2019, **209**: 811-829.

[28] TANG Y, DING Q. Nonlinear vibration analysis of a bi-directional functionally graded beam under hygro-thermal loads[J]. *Composite Structures*, 2019, **225**: 111076.

[29] BARATI A, HADI A, NORROZI R, et al. On vibration of bi-directional functionally graded nanobeams under magnetic field[J]. *Mechanics Based Design of Structures and Machines*, 2020, **50**(2): 468-485.

[30] HUANG Y, OUYANG Z Y. Exact solution for bending analysis of two-directional functionally graded Timoshenko beams[J]. *Archive of Applied Mechanics*, 2020, **90**: 1005-1023.

[31] WATTANASAKULPONG N, UNGBHAKORN V. Linear and nonlinear vibration analysis of elastically restrained ends FGM beams with porosities[J]. *Aerospace Science and Technology*, 2014, **32**(1): 111-120.

[32] SHAFIEI N, MIRJAVADI S S, RABBY B, et al. Vibration of two-dimensional imperfect functionally graded (2D-FG) porous nano-/micro-beams[J]. *Computer Methods in Applied Mechanics and Engineering*, 2017, **322**: 615-632.

[33] ZHANG B, HE M, LIU D, et al. Size-dependent functionally graded beam model based on an improved third-order shear deformation theory[J]. *European Journal of Mechanics A: Solids*, 2014, **47**: 211-230.

[34] ŞIMŞEK M. Fundamental frequency analysis of functionally graded beams by using different higher-order beam theories[J]. *Nuclear Engineering and Design*, 2010, **240**(4): 697-705.

[35] AKGÖZ B, CIVALEK Ö. Free vibration analysis of axially functionally graded tapered Bernoulli-Euler microbeams based on the modified couple stress theory[J]. *Composite Structures*, 2013, **98**: 314-322.